

## Research Article

Jianhua Xiao\*, Ru Yang, Shiqiang Song, Haibin Wang, and Haiwei Wen

# Effect of capillary arrays on the profile of multi-layer micro-capillary films

<https://doi.org/10.1515/epoly-2023-0022>

received August 02, 2023; accepted August 23, 2023

**Abstract:** Multi-layer micro-capillary films (MCFs) have broad application prospects in the micro-fluid field. These films consist of two-dimensional arrays of hollow microcapillaries. The arrangements of hollow microcapillary arrays in extrusion die strongly influence the shape and size of multi-layer MCFs. However, most of the studies focus on a single-layer film. In this study, the models of multi-layer MCF extrusion die with hollow capillary arrays from one layer to four layers have been modeled. Numerical simulations show that when the hollow capillary arrays in different layers are aligned, the aspect ratio of the capillary is smaller and the flow resistance is small, so this kind of multi-layer MCF is suitable for micro-reactor and melt pump. When the hollow capillary arrays in different layers are non-aligned, the aspect ratio of the capillary is relatively larger and the specific surface is bigger, so this kind of multi-layer MCF has a high capability of heat exchange and is suitable for micro heat exchangers.

**Keywords:** micro-capillary, multi-layer MCF model, hollow microcapillary arrays, aspect ratio of capillary

## 1 Introduction

Micro-capillary film (MCF) extrusion is a novel process for the manufacturing of continuous MCFs. It was put forward by Hallmark (1,2) in 2003. In this process (B. Hallmark, April 2007, Apparatus and method for producing a film having a tear guiding region, and an extruded film having

such a tear guided region, U.S. patent 20080248147A1), the polymer is extruded through an array of hollow extrusion die. Then, in the holes of the extrusion die, a high-pressure gas is injected into the polymer melt to form continuous MCFs (Figure 1).

The low density polyethylene (LDPE) film, polyvinylidene fluoride film, and fluorinated ethylene propylene copolymer film with 19-, 42- (3), or 10 capillaries have been fabricated with 30–500  $\mu\text{m}$  capillaries (4). The advantages of MCFs include thin walls, good optical properties, large A/V, small capillary diameter, plug flow, multi-capillaries, simple fluidics, disposability, and low cost. They have potential applications in photonics heat exchange, non-invasive tracking, adsorbent material, fast kinetics, bioprocessing, and micro-reactor technology.

The MCF can be effectively used for micro-heat exchanger, micro reactions, and bioprocessing. The efficacy of heat transfer of the MCF is close to metallic microfluidic devices (5). It provides an effective means of either heating or cooling fluids, or removing heat from a hot surface (6). It has been successfully used to fabricate plastic solar collectors (7) and made into spirals or solid discs adopted in microreactors (8).

The MCF can also be effectively used for micro-flow, drug delivery (NS Grasman, Microcapillary polymer films for drug delivery, May 2017, US patent 20170119692A1), mass transfer, and purification. The fluid flow in a capillary tube exhibits high-performance “plug” features (9). It can be designed for miniaturized microfluidic biosensing devices (10), CECs in water, and viruses and bacteria removal devices (11), phase change materials (R J Koopmans, MCFs containing phase change materials, Jan 2013, US patent 20140113112A1), and superparamagnetic nanoparticle purification (12). The purities are typically more than 95% (13).

The MCF can also be used in bioanalytical techniques, such as rapid point-of-care quantitation of bacterial (14), semi-quantitative determination of hydrogen peroxide (15), protein chromatography, multiplex immunoassays (16), and fluorescence immunoassay quantitation of *Escherichia coli* optical microfluidic test (17).

However, in the aforementioned studies, the MCF is a single-layer film. A multi-layer MCF has higher mechanical strength than the single-layer MCF. It has potential prospective

\* **Corresponding author: Jianhua Xiao**, School of Chemistry and Chemical Engineering, Shanghai University of Engineering Science, Shanghai 201620, China, e-mail: 04200010@sues.edu.cn

**Ru Yang, Shiqiang Song:** School of Chemistry and Chemical Engineering, Shanghai University of Engineering Science, Shanghai 201620, China

**Haibin Wang, Haiwei Wen:** School of Materials Science Engineering, Nanchang Hangkong University, Nanchang 330000, China

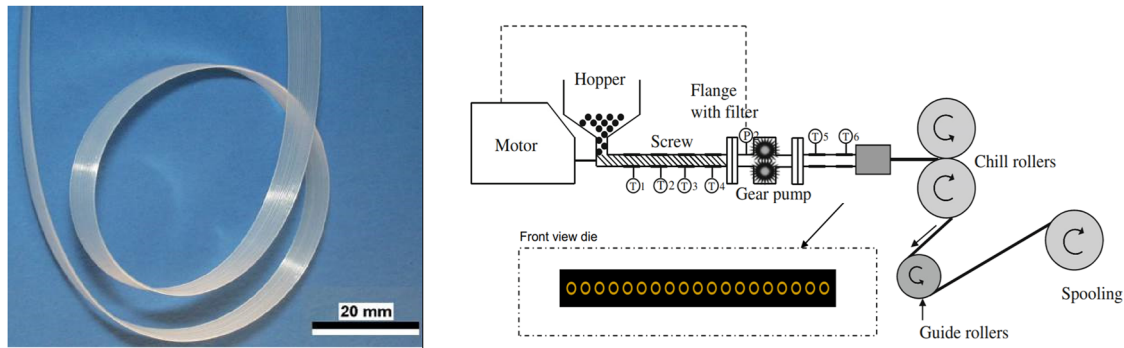


**Figure 1:** MCFs and the MCF extrusion process.

applications in biomedical, life science, engineering science, and physical science. It has been fabricated by heat melting of multiple single-layer MCFs to form MCF monoliths (18). Some patents introduced an extrusion die for manufacturing multi-layer MCFs (D Joseph, 7 Nov 2018, System and method for producing a multi-layer MCF, EP Patent 2867000B1). However, the influence of the arrangement of capillary arrays on the shape and size of the external film has not been studied systematically. In this study, the numerical simulation method is adopted to study the multi-layer MCF extrusion process.

Section 1 describes the development, process, and application of an MCF. Section 2 details the modeling, meshing, rheological parameters, constitutive equations, and boundary conditions used in the numerical simulation of multiple-layer MCFs with typical 9 capillaries in the same

layer. Section 3 discusses the effect of the arrangement of capillary arrays on the shape and size of the external film or internal capillary within single- and multi-layer MCF.

## 2 Numerical simulation

### 2.1 Models of single- and multi-layer MCFs

The cross section of single- and multi-layer MCF models modeled in this study have nine types of hollow capillary arrays from one layer to four layers (Figure 2). Some capillary arrays in different layers are aligned, and some of them are non-aligned.

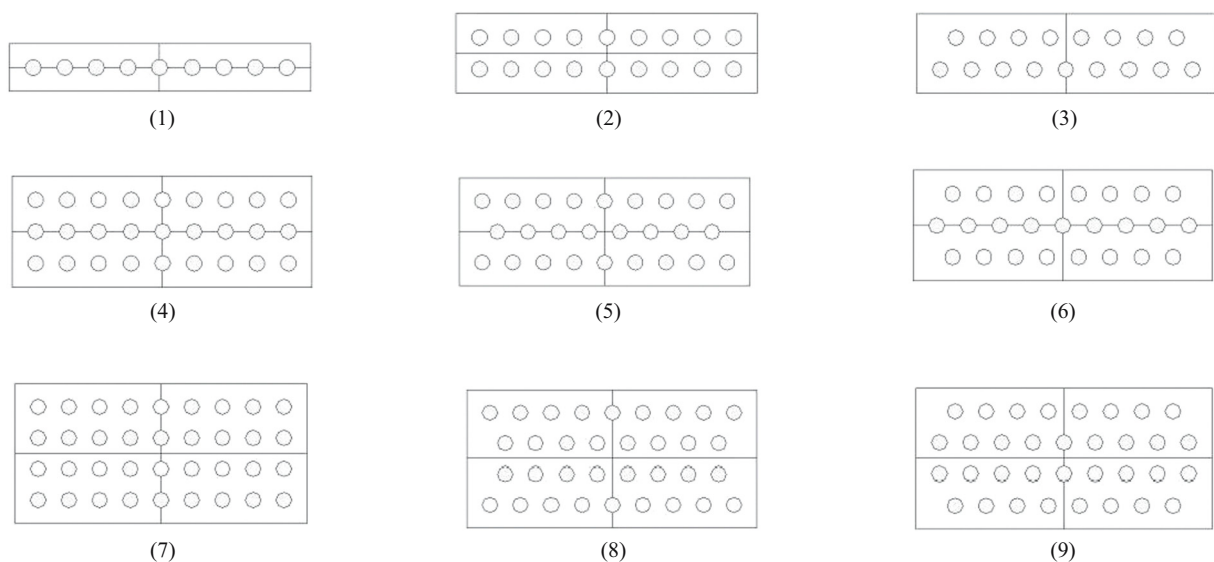


**Figure 2:** Cross section of single- and multi-layer MCF models with different capillary arrays. (1) Single-layer MCF with 9 capillaries. (2) Bi-layer MCF with 18 capillaries. (3) Bi-layer MCF with 17 capillaries. (4) Three-layer MCF with 27 capillaries. (5) Three-layer MCF with 26 capillaries. (6) Three-layer MCF with 25 capillaries. (7) Four-layer MCF with 36 capillaries. (8) Four-layer MCF with 16 capillaries in the middle. (9) Four-layer MCF with 18 capillaries in the middle.

The diameter of the capillaries is 0.50 mm, and the spacing between capillaries is 0.50 mm. The width of the models is 9.50 mm. The thickness of the MCF model, shown in Figure 2(1), (3), (4)–(6), and (7)–(9), are 1.50, 2.50, 3.50, and 4.50 mm, respectively.

The 3D models were established (Figure 3). There are outer and inner domains in the models: one domain represents inside the extrusion die (length = 2 mm), and the other domain represents outside the die (length = 7 mm). 1/4 bisymmetric axis models are used for saving the CPU-solving times.

Detailed information on MCF models is shown in Table 1. Porosity is the ratio of the area of capillaries on the cross section to the area of the whole MCF film. From single-layer to four-layer MCF with capillaries aligned, the porosities are 12.39, 14.87, 15.93, and 16.52%. Under the same layer numbers, the films with aligned capillaries have more holes than nonaligned capillaries. The number of meshes for each model is about 10,000. The geometric models were meshed using Gambit software.

## 2.2 Material parameters

In this work, a generalized Newtonian constitutive equation, the Carreau–Yasuda model in Eq. 1 is used to describe LDPE rheology:

$$\eta(\dot{\gamma}) = \eta_{\infty} + (\eta_0 - \eta_{\infty})[1 + (\lambda\dot{\gamma})^a]^{-\frac{n-1}{a}} \quad (1)$$

where  $\eta_0$  and  $\eta_{\infty}$  are the shear viscosities at zero and high shear rates, respectively;  $\dot{\gamma}$  is the shear rate;  $\lambda$  is the relaxation time;  $a$  is the material data; and  $n$  is a non-Newtonian index. This model is suitable for the description of the viscosity functions in the terminal and in the shear-thinning regime:  $\eta_0 = 13,800$  Pa·s,  $n = 0.34$ ,  $a = 0.93$ , and  $\lambda = 0.17$  s (19).

## 2.3 Boundary condition sets

Boundary conditions inflow, wall, free surface, outflow, and plane of symmetry are set in Ansys software. The

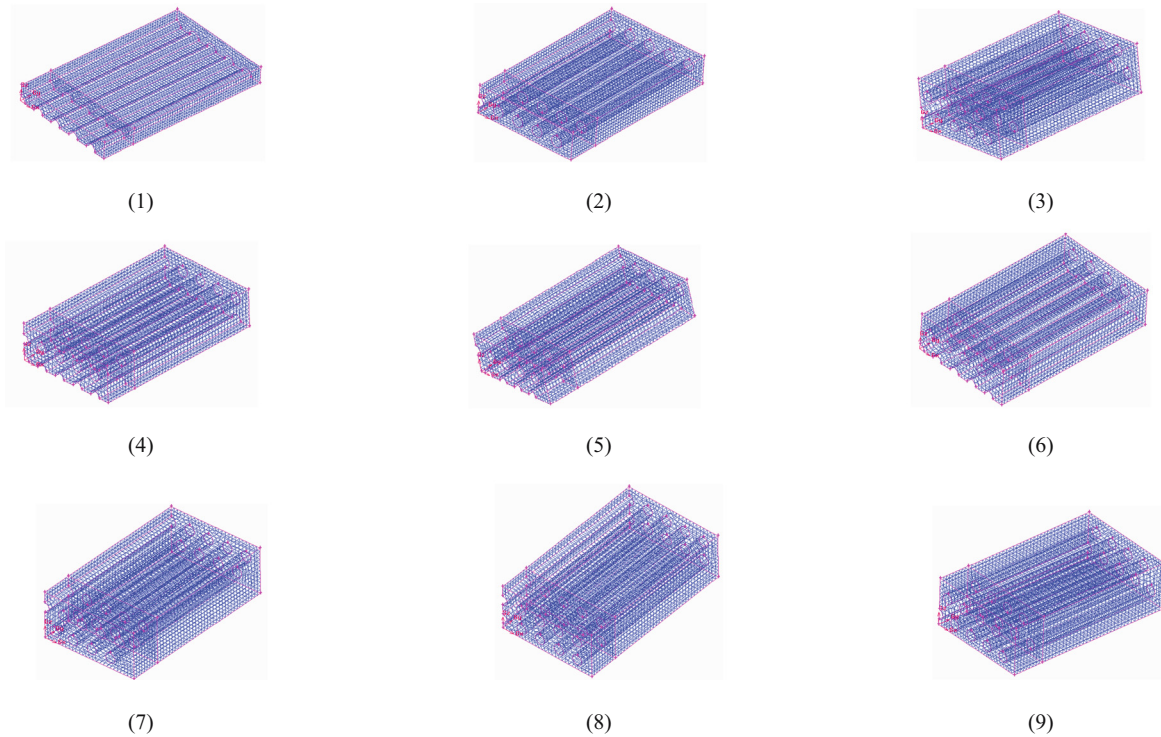


**Figure 3:** 1/4 bisymmetric axis model and mesh of single- and multi-layer MCF models. (1) Single-layer MCF with 9 capillaries. (2) Bi-layer MCF with 18 capillaries. (3) Bi-layer MCF with 17 capillaries. (4) Three-layer MCF with 27 capillaries. (5) Three-layer MCF with 26 capillaries. (6) Three-layer MCF with 25 capillaries. (7) Four-layer MCF with 36 capillaries. (8) Four-layer MCF with 16 capillaries in the middle. (9) Four-layer MCF with 18 capillaries in the middle.

**Table 1:** Width, thickness, porosity, and mesh node of single- and multi-layer MCF models

Model	MCF	Width (mm)	Thickness (mm)	Capillary number	Capillary array	Porosity of die (%)	Mesh node	Solving time (s)
1	Single-layer MCF with 9 capillaries	9.50	1.50	9	Aligned	12.39	10,125	1,353
2	Bi-layer MCF with 18 capillaries	9.50	2.50	18	Aligned	14.87	10,107	2,477
3	Bi-layer MCF with 17 capillaries	9.50	2.50	17	Non-aligned	14.04	13,392	4,821
4	Three-layer MCF with 27 capillaries	9.50	3.50	27	Aligned	15.93	11,241	1,876
5	Three-layer MCF with 26 capillaries	9.50	3.50	26	Non-aligned	15.34	13,872	1,942
6	Three-layer MCF with 25 capillaries	9.50	3.50	25	Non-aligned	14.76	10,116	2,147
7	Four-layer MCF with 36 capillaries	9.50	4.50	36	Aligned	16.52	13,833	3,167
8	Four-layer MCF with 16 capillaries in the middle	9.50	4.50	34	Non-aligned	15.60	13,338	7,106
9	Four-layer MCF with 18 capillaries in the middle	9.50	4.50	34	Non-aligned	15.60	13,545	15,305

inflow boundary is a fully developed flow with a total volumetric flow rate of  $5 \text{ cm}^3\text{s}^{-1}$ . At each end of the model, a stretch force has been exerted. The geometric model and boundary conditions of the two-layer MCF are shown in Figure 4, and the same boundary conditions are set in all nine models.

### 3 Results and discussion

A 3D adaptive remeshing technique was applied to the whole domain of free surface remeshing. Considering the extrusion swelling phenomenon and the deformation of stretching force exerted, and ensuring convergence of calculation and increasing the calculating speed, appropriate assumptions are made to reduce the non-linearity of the simulation: (1) the steady-state process in the melt drawing stage is isothermal; (2) the melt flow on the micro-capillary wall is no-slip flow, i.e., each velocity component is zero on the wall; (3) the fluid flow in the inlet of the calculation region is fully developed; and (4) density and the surface tension are neglected.

#### 3.1 Film shape and size

##### 3.1.1 Film shape

The molten polymer is extruded through a die. The whole shapes of the multi-layer MCF in the die and outside the die are shown in Figure 5.

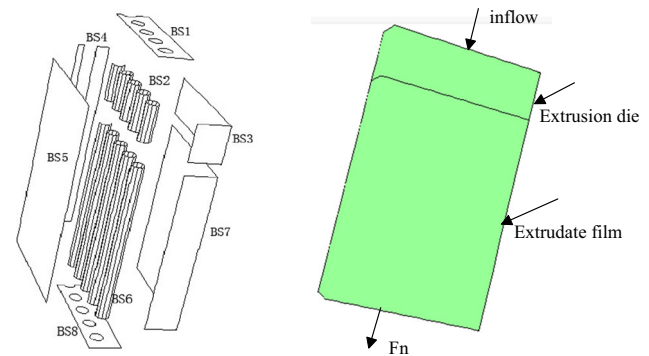


**Figure 4:** 1/4 bisymmetric axis model of the bi-layer MCF with 18 capillaries used in the simulation. BS1 is the inflow,  $Q = 5 \text{ cm}^3\text{s}^{-1}$ . BS2 and BS3 are, respectively, identified as the wall of the gas injection die and polymer extrusion dies.  $V_n = 0$  and  $V_s = 0$ . BS4 and BS5 are planes of symmetries,  $V_n = 0$  and  $F_s = 0$ . BS6 and BS7 are the free surfaces that are outside the die,  $V_n = 0$  and  $F_n = 0$ . BS8 is the place where the stretching force acts.  $F_n = 3 \text{ N}$ ,  $V_n$  is the normal velocity,  $V_s$  is the tangential velocity,  $F_n$  is the normal force, and  $F_s$  is the tangential force.



From the numerical simulation results, every model is obviously divided into two subdomains, one is inside of the die and the other is outside of the die. At the end of the MCF, a stretch force is exerted. Under the action of normal force, the shape and the size of the MCF have been changed.

The upper and lower surfaces of the MCF inside the die are both flat, while the upper and lower surfaces outside the die are waved. This is because the die-swell effect of the polymer makes the surface of the MCF film contract and

expand in different parts. As shown in Figure 5a, b, d, and g, the hollow capillary arrays are aligned. The upper and lower surfaces of the MCF are slightly waved. As shown in Figure 5c, e, f, h, and i, the hollow capillary arrays are non-aligned. The end of the upper and lower surfaces has obviously warpage deformation, especially as shown in Figure 5f, h, and i.

The sides of the MCF film are also not flat. As shown in Figure 5a, b, d, and g, they are slightly wavy. However, as shown in Figure 5c, e, and h, they are obviously swelled,

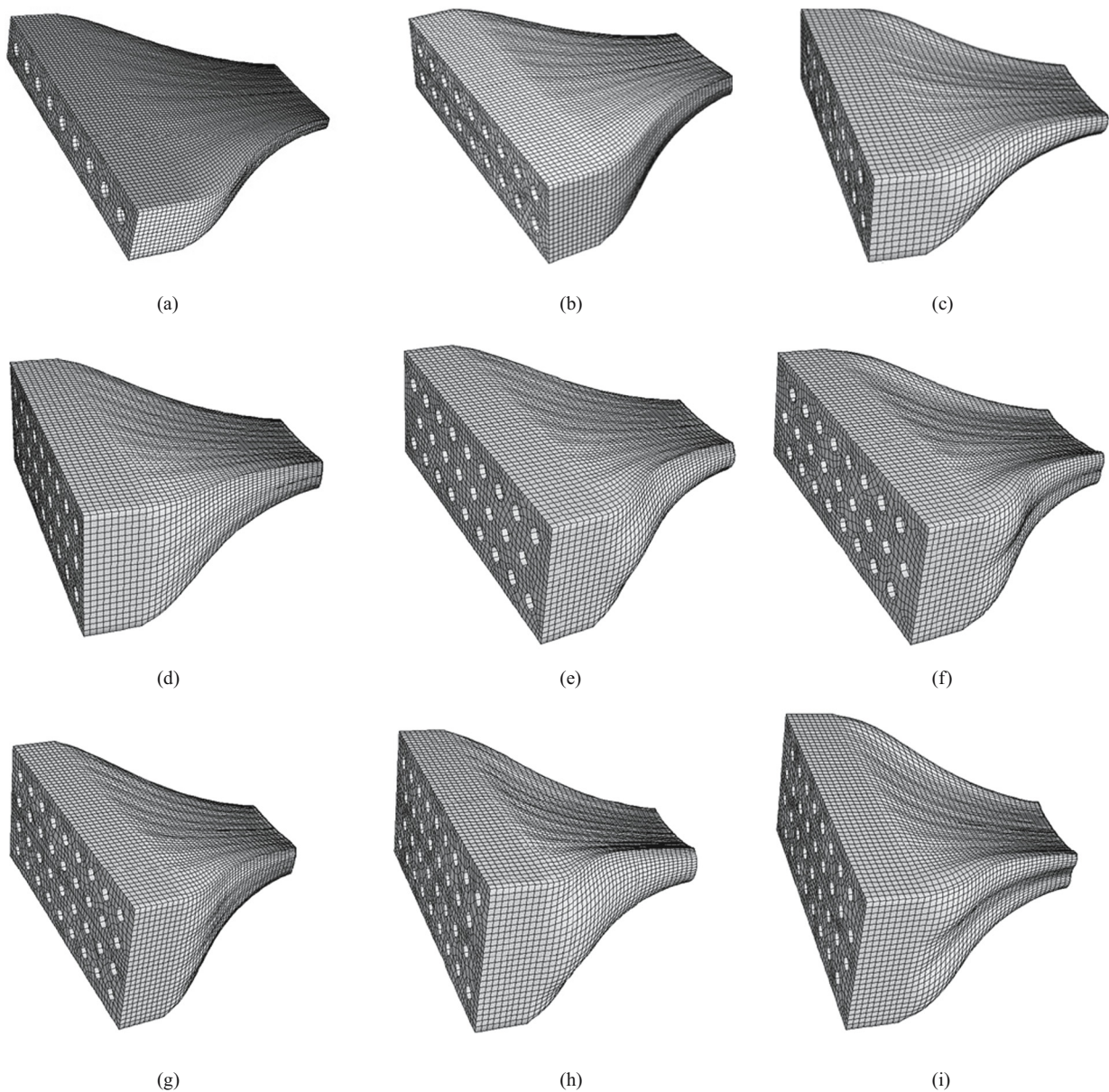


**Figure 5:** The shape of the multi-layer MCF in the extrusion die and outside the die. (a) Single-layer MCF with 9 capillaries. (b) Bi-layer MCF with 18 capillaries. (c) Bi-layer MCF with 17 capillaries. (d) Three-layer MCF with 27 capillaries. (e) Three-layer MCF with 26 capillaries. (f) Three-layer MCF with 25 capillaries. (g) Four-layer MCF with 36 capillaries. (h) Four-layer MCF with 16 capillaries in the middle. (i) Four-layer MCF with 18 capillaries in the middle.

while, in Figure 5f and i, they are obviously sunk. From the whole modeling, including the upper and side surfaces, the shape of the multi-layer MCF with hollow capillaries and aligned arrangement will be closer to the shape of the extrusion die. While the shapes of the multi-layer MCF with hollow capillaries and non-aligned arrangement are seriously deformed. Therefore, the hollow capillary array has a great effect on the shape of the multi-layer MCF.

### 3.1.2 Film size

The width and thickness of the single and multi-layer MCF were smaller under the effect of a 3 N stretching force. Detailed data are shown in Table 2.

Table 2 shows the width and thickness of the die size and film size in the nine types of MCF models under a stretch force of 3 N. In the nine models, from one to four layers, the shrinkage of the width increases from 64% to 67%, and the shrinkage of the thickness increases from 68% to 74%. In the same layer models, more capillaries have higher shrinkage in size. In models h and i, the polymer content is the same but the shrinkage is different. It is because the warpage deformation caused by the polymer swell leads to a change in the film shape and film size.

The aspect ratio of the MCF die ( $A_{die}$ ) is the width to thickness of the MCF extrusion die in Eq. 2. Similarly, the aspect ratio of the MCF film ( $A_{film}$ ) is the width to thickness of the extrudate film in Eq. 3.  $A_{die}$  and  $A_{film}$  are the profile parameters of the multi-layer MCF before and after stretching in this study:

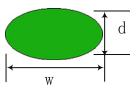
$$A_{die} = \frac{W_{die}}{Th_{die}} \quad (2)$$

$$A_{film} = \frac{W_{film}}{Th_{film}} \quad (3)$$

$A_{die}$  is a constant value in the nine types of models of the extrusion die. However, as shown in Figure 6c, the  $A_{film}$  value is not the same in the nine types of models because the polymer swell and porosity are different in these nine models.  $A_{film}/A_{die}$  is the ratio of the width to thickness of the MCF before and after stretching. Figure 6c shows that  $A_{film}/A_{die}$  changes from 1.17 to 1.28 in the nine models. All  $A_{film}/A_{die}$  values are greater than 1, because of the application of a stretch force at the end of the films, and the  $A_{film}/A_{die}$  values are higher when the two-dimensional hollow capillaries are arranged regularly and orderly.

## 3.2 Capillary shape and size

Under the action of a tensile force, the shape and size of the MCF and capillaries are changed. The inter-capillary aspect ratio is of the width to depth and  $A_{capillary}$  is greater than or equal to 1.



$$A_{capillary} = \frac{W}{d} \quad (A_{capillary} \geq 1)$$

### 3.2.1 Single-layer MCF

As shown in Figure 7a, the shape of the external film and the internal capillary in a single-layer MCF are changed after stretching. In the extrusion die (before stretching), the internal capillary is all circle. The model is meshed by a triangle grid and uses the nonlinear densification technology. After the melt leaves the die, the film becomes thin and narrow under the action of a stretch force, and the internal capillary shapes are no longer circular. The inter-capillary aspect ratios are shown in Figure 7b. The internal aspect ratios of the capillaries located on both sides of the MCF film are nearly 1, i.e., the deformation

**Table 2:** Size shrinkage of the width and thickness in the multi-layer MCF under a stretch force of 3 N

Model	Width			Thickness			$A_{die}$	$A_{film}$	$A_{film}/A_{die}$
	Die size (mm)	Film size (mm)	Shrinkage (%)	Die size (mm)	Film size (mm)	Shrinkage (%)			
1	9.50	3.22	66	1.50	0.40	73	6.33	8.05	1.27
2	9.50	3.22	66	2.50	0.66	74	3.80	4.88	1.28
3	9.50	3.37	65	2.50	0.75	70	3.80	4.49	1.18
4	9.50	3.16	67	3.50	0.91	74	2.71	3.47	1.28
5	9.50	3.34	65	3.50	0.99	72	2.71	3.37	1.24
6	9.50	3.75	66	3.50	1.12	68	2.71	3.35	1.23
7	9.50	3.11	67	4.50	1.19	74	2.11	2.61	1.24
8	9.50	3.36	65	4.50	1.30	71	2.11	2.58	1.22
0	9.50	3.38	64	4.50	1.37	70	2.11	2.46	1.17

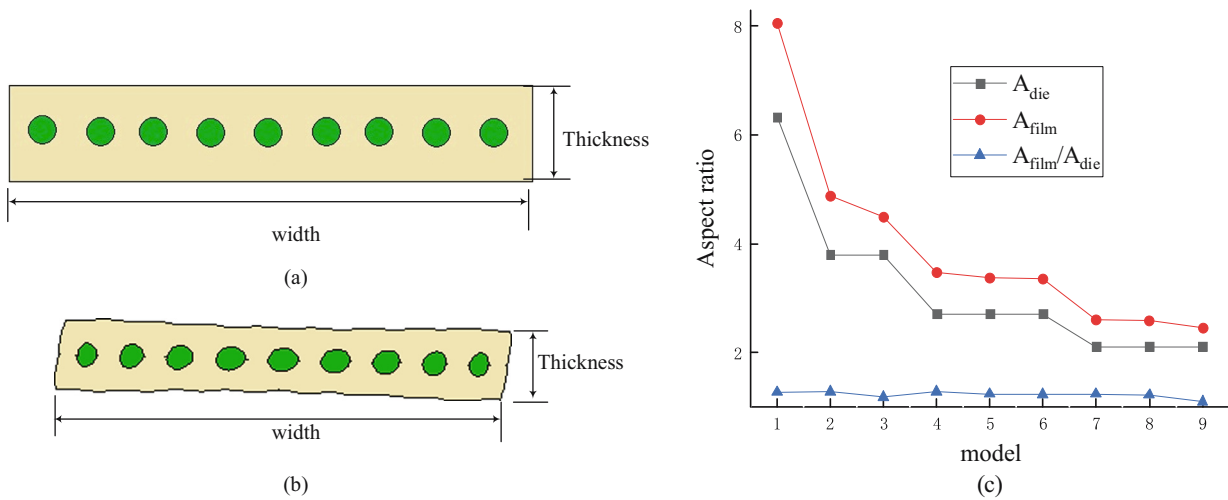


**Figure 6:**  $A_{die}$  and  $A_{film}$  in nine MCF models. The size of the (a) extrusion die and (b) MCF film and (c)  $A_{die}$  and  $A_{film}$ , and  $A_{film}/A_{die}$ .

of the capillaries is small. The internal aspect ratio of the capillary in the central is the largest.

### 3.2.2 Bi-layer MCF

As shown in Figure 8, the shape and size of the external film and internal capillary in the bi-layer MCF with 18 or 17 capillaries have changed after stretching. After the polymer melt

leaves the die, the film becomes thin and narrow under the action of a stretch force; its four surfaces (including upper, down, left, and right) are no longer flat and the capillary shapes are no longer circular. As shown in Figure 8b, on the upper left and upper right, there are two corners with an obvious swell because of the viscoelasticity of the polymer.

The inter-capillary aspect ratio of the bi-layer MCF is shown in Figure 8c and d. The inter-capillary aspect ratio in the bi-layer MCF with 17 holes is higher than that in the

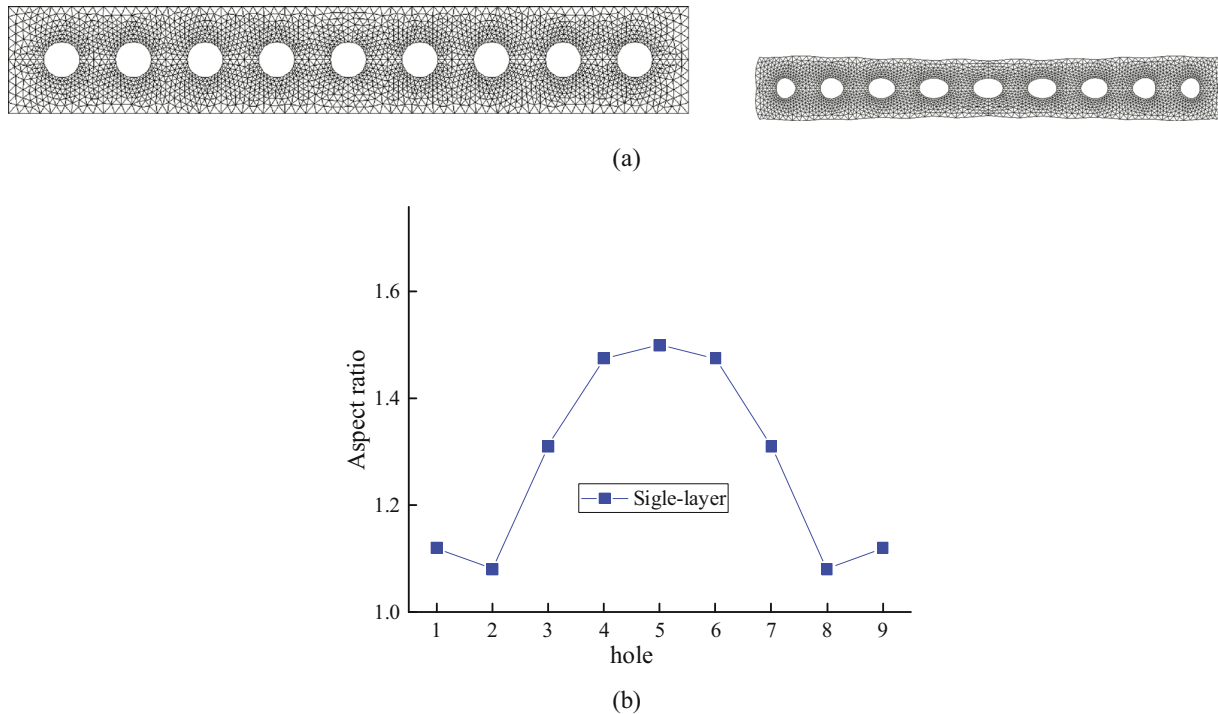


**Figure 7:** The cross section of a single-layer MCF before and after stretching, and aspect ratios of all holes. (a) Single-layer MCF with nine holes before and after stretching. (b) Inter-capillary aspect ratios of the single-layer MCF.

bi-layer MCF with 18 holes and the aspect ratio of 11 capillaries is stable near 1.6. This shows that the two-dimensional hollow capillary array has a great effect on all hole shapes.

In the bi-layer MCF with 18 capillaries, the inter-capillary aspect ratio in the first layer is the same as in the second layer. In the same layer, the inter-capillary aspect ratio is higher in the central and lower on the two sides. From the central to the side, the aspect ratio decreases. But in the bi-layer MCF with 17 capillaries, the first layer has 8 holes, and the second layer has 9 holes. So, the inter-capillary aspect ratio in the first layer is different from the second layer.

### 3.2.3 Three-layer MCF

The cross section of the three-layer MCF before and after stretching and the inter-capillary aspect ratio of all holes are shown in Figure 9.

As shown in Figure 9, all the surfaces (upper, down, left, and right) in the three-layer MCF are not flat: in Figure 9b, it looks like a drum, and in Figure 9c, it looks like a dog bone shape. This shows that the two-dimensional hollow capillary array has a great effect on the film shape and film size.

The aspect ratios of the internal capillaries are shown in Figure 9d–f. The inter-capillary aspect ratios in the

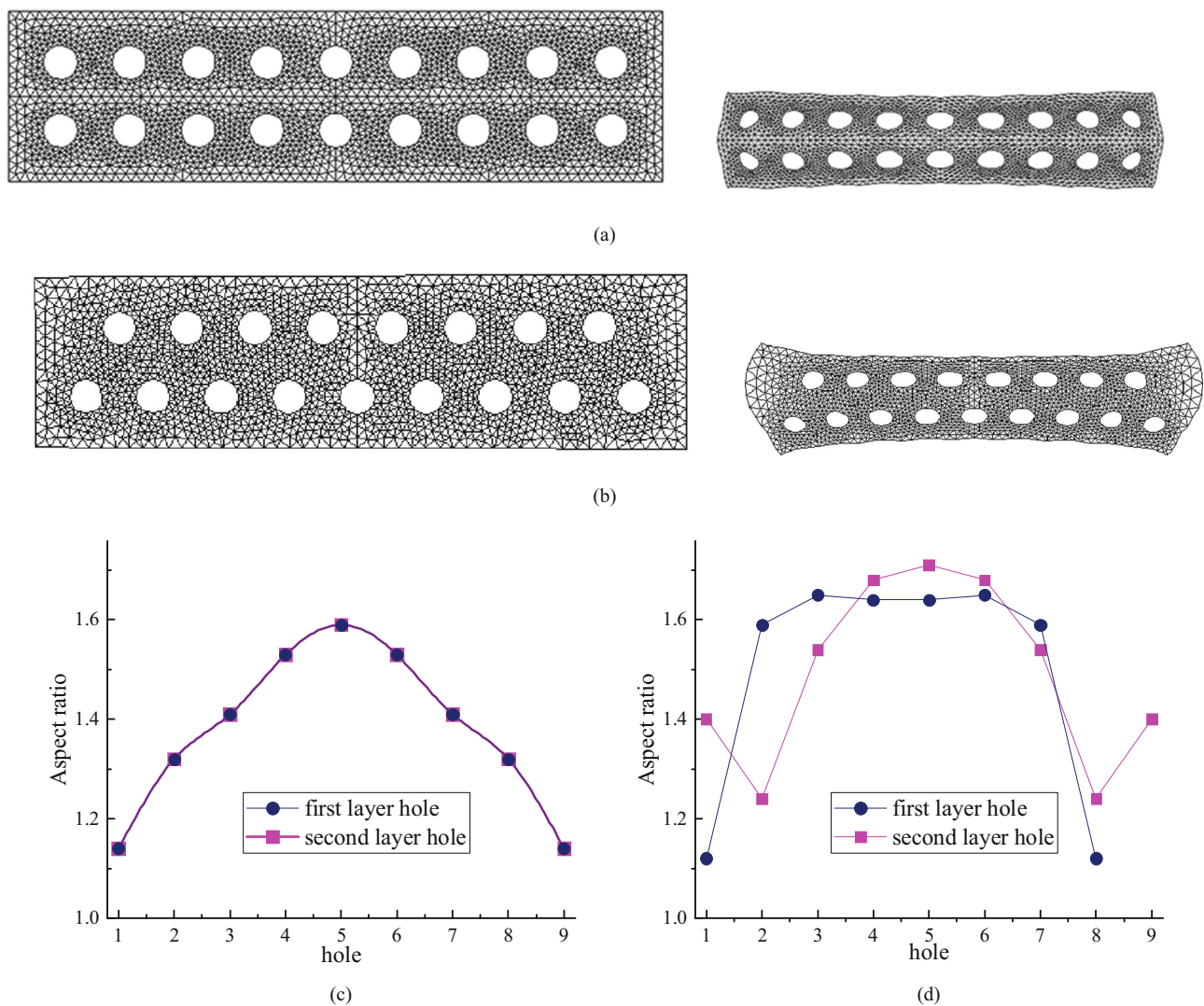


**Figure 8:** The cross section of the bi-layer MCF before and after stretching and the aspect ratios of all holes. (a) The bi-layer MCF with 18 holes before and after stretching. (b) Bi-layer MCF with 17 holes before and after stretching. Inter-capillary aspect ratios of the single-layer MCF with (c) 18 holes and (d) 17 holes.



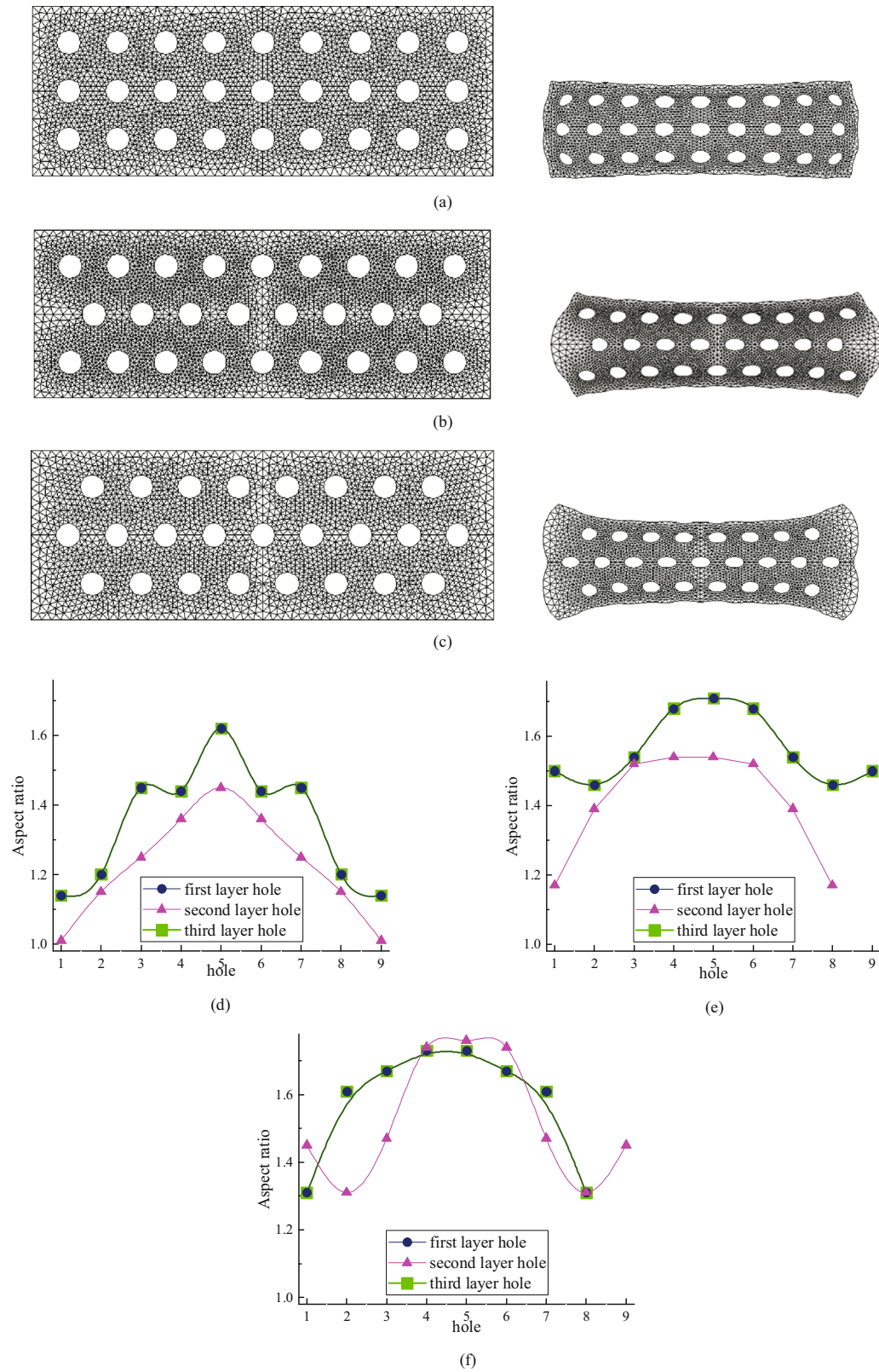


**Figure 9:** The cross section of the three-layer MCF before and after stretching, and the aspect ratios of all holes. (a) Three-layer MCF with 27 holes before and after stretching. (b) Three-layer MCF with 26 holes before and after stretching. (c) Three-layer MCF with 25 holes before and after stretching. Aspect ratios of the internal capillaries with (d) 27 holes, (e) 26 holes, and (f) 25 holes.



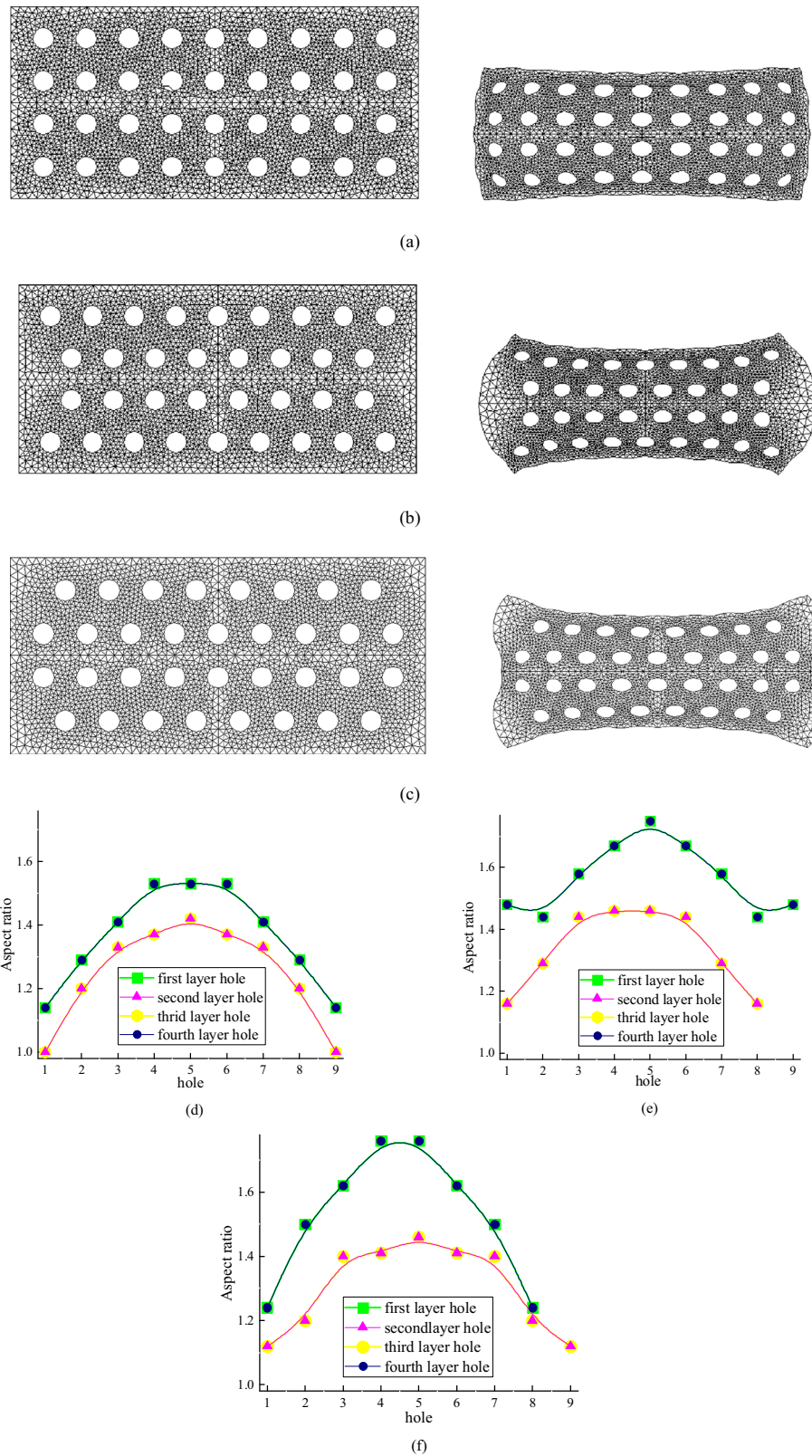


**Figure 10:** The cross section of the four-layer MCF before and after stretching, and the aspect ratios of all holes. (a) Four-layer MCF with 36 holes before and after stretching. Four-layer MCF with 34 holes before and after stretching, and the numbers of holes in middle layers are (b) 16 holes, (c) 18 holes. Aspect ratios of the internal capillaries with (d) 36 holes, (e) 34 holes (16 holes in the middle), and (f) 34 holes (18 holes in the middle).

three-layer MCF with 26 and 25 capillaries are higher than that of the three-layer MCF with 27 capillaries.

In the three-layer MCF with 25, 26, and 27 capillaries, the inter-capillary aspect ratio in the first layer is the same as the third layer but higher than the middle layer. The aspect ratio is higher in the central and lower on the two sides in all layers. In the three-layer MCF with 25 capillaries, the inter-capillary aspect ratio values with capillaries are higher than 1.6; in the three-layer MCF with 26 capillaries, the inter-capillary aspect ratio values with 6 capillaries are higher than 1.6; and in three-layer MCF with 27 capillaries, the inter-capillary aspect ratio with only 2 capillaries is higher than 1.6. The highest value of  $A_{\text{capillary}}$  is 1.76, it appears in the 25-capillary film. The lowest value of  $A_{\text{capillary}}$  is 1.01, and it appears in the 27-capillary film.

### 3.2.4 Four-layer MCF

The cross sections of the four-layer MCF before and after stretching are shown in Figure 10. As shown in Figure 10b, it looks like a drum, and in Figure 10c it looks like a dog bone. The inter-capillary aspect ratios are also shown in Figure 10d–f. The inter-capillary aspect ratios in the four-layer MCF with 16 and 18 capillaries in the middle are higher than that of the four-layer MCF with 36 capillaries.

In the four-layer MCF, the inter-capillary aspect ratios in the first layer are the same as in the fourth layer, and the inter-capillary aspect ratios in the second layer are the

same as in the third layer. The inter-capillary aspect ratios are bigger in the first and fourth layers but lower in the second and third layers. In the four-layer MCF with 16 capillaries in the middle, the inter-capillary aspect ratios with about 10 holes are higher than 1.6. In the four-layer MCF with 18 capillaries in the middle, the aspect ratio values with about 8 holes are higher than 1.6. In the four-layer MCF with 36 capillaries, no aspect ratio values are higher than 1.6.

### 3.3 Effects of two-dimensional hollow capillary array on the flow efficiency of the MCF

The geometric models of the multi-layer MCF belong to the bi-axial symmetric geometric model. In order to avoid data duplication, a 1/4 geometric model is taken to investigate the influence of the capillary arrays on the effect of the multi-layer MCF. The results are shown in Table 3.

Every capillary is elliptical in shape or oval. As a result, an equivalent radius,  $R_{\text{eq}}$  (20), was calculated from Eq. 4 and used to indicate the actual capillary radius. In Eq. 4,  $a$  and  $b$  are the major and minor semi-axes of the ellipse, respectively.  $N$  is the number of the holes. The area of all the elliptical holes can be calculated by Eqs. 5 and 6.  $A_{\text{cs}}$  is the cross-sectional area of the MCF film, which is calculated with the Ansys software. The porosity of the film is the ratio of all the elliptical hole areas to the whole cross-sectional area (Eqs. 7 and 8):

**Table 3:** Relationship between the capillary arrays and the average of  $A_{\text{capillary}}$  and porosity in the multi-layer MCF

Model	Capillary array	Hole layer	Aspect ratios of internal capillaries						Porosity film (%)		
			1	2	3	4	5	Average	$P_{f1}$	$P_{f2}$	Average
1	Aligned	1	1.12	1.08	1.31	1.48	1.50	1.30	13.6	13.4	13.5
2	Aligned	1	1.14	1.32	1.41	1.53	1.59	1.40	16.1	15.7	15.9
3	Non-aligned	1	1.40	1.24	1.51	1.68	1.71	1.50	13.8	13.3	13.6
4	Aligned	2	1.12	1.59	1.65	1.64	—	1.34	18.4	17.2	17.8
		1	1.14	1.20	1.45	1.44	1.62				
5	Non-aligned	2	1.01	1.50	1.25	1.36	1.45	1.49	16.1	15.5	15.8
		1	1.50	1.46	1.54	1.68	1.71				
6	Non-aligned	2	1.17	1.39	1.52	1.54	—	1.56	15.6	14.4	15.0
		1	1.31	1.61	1.67	1.73	—				
7	Aligned	2	1.45	1.31	1.47	1.74	1.76	1.32	18.3	18.0	18.2
		1	1.14	1.29	1.41	1.53	1.53				
8	Non-aligned	2	1.00	1.20	1.33	1.37	1.42	1.46	16.5	16.0	16.3
		1	1.48	1.44	1.58	1.67	1.75				
9	Non-aligned	2	1.16	1.29	1.44	1.46	—	1.43	16.6	16.2	16.4
		1	1.24	1.50	1.62	1.76	—				
		2	1.12	1.20	1.40	1.41	1.46				
		1									

$$R_{eq} = \left( \frac{32 \cdot a^3 \cdot b^3}{a^2 + b^2} \right)^{0.25} \cdot \frac{1}{2} \quad (4)$$

$$S_1 = \sum_{i=1}^n \pi R_{eq}^2 \quad (5)$$

$$S_2 = \sum_{i=1}^n \pi ab \quad (6)$$

$$P_{f1} = \frac{S_1}{A_{cs} + S_1} \times 100\% \quad (7)$$

$$P_{f2} = \frac{S_2}{A_{cs} + S_2} \times 100\% \quad (8)$$

As shown in Table 3, the aspect ratios of the internal capillaries range from 1.01 to 1.76. The porosity of the film ranges from 13.5% to 18.2%. Under the conditions of the same layer, when the capillary array is aligned, the porosity of the MCF is high and the capillary aspect ratio is small. When the capillary array is non-aligned, the porosity of the MCF is small and the aspect ratio of the capillary is relatively higher.

The flow efficiency of the multi-layer MCF depends on two factors: flow resistance and specific surface area. When the aspect ratio of the capillaries is close to 1, the shape is close to circular, and the flow resistance is the minimum under the same volume flow rate. When the aspect ratio of the capillaries is far away from 1, the specific surface area is the maximum under the same

volume, and the heat exchange is also the maximum. If the multi-layer MCF is used for fluid transportation, such as the micro melt pump and microreactor, the multi-layer MCF with aligned capillary arrays should be chosen. It is very beneficial for reducing fluid resistance and improving fluid transmission efficiency. If the multi-layer MCF is used for exchange energy, such as a micro heat exchanger, the multi-layer MCF with a non-aligned capillary array should be chosen.

The function of the multi-layer MCF depends on two important parameters: the film porosity and the capillary aspect ratio. The aligned four-layer MCF film has the highest film porosity and the smallest capillary aspect ratio in the multi-layer MCF. It is very beneficial for reducing fluid resistance and improving fluid transmission efficiency. So, the aligned four-layer MCF film is suitable for use for fluid transportation, such as micro melt pumps and microreactors. In order to improve the efficiency of microheat exchangers, MCF should have higher film porosity and a higher capillary aspect ratio. In multi-layer MCF films, non-aligned MCFs have a higher capillary aspect ratio than their arranged MCFs. The three/four-layered MCF film arranged in a non-aligned manner has higher film porosity than the two-layer MCF. It is best to choose three/four-layer MCF films arranged in a non-aligned manner for energy exchange, such as micro heat exchangers (Figure 11).

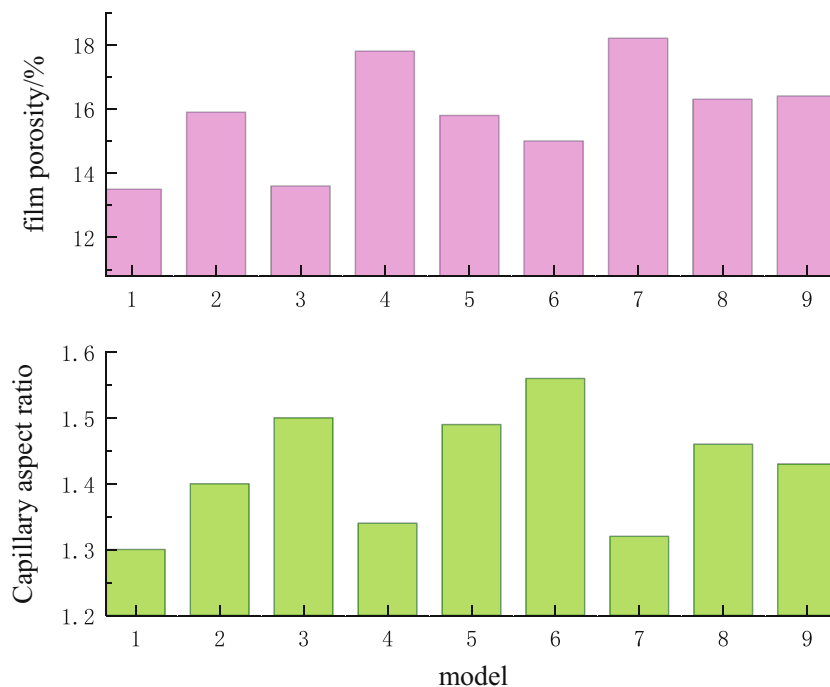


Figure 11: Film porosity and capillary aspect ratio in the nine models.

## 4 Conclusions

Under the conditions of the inlet flow rate  $Q = 5 \text{ cm}^3 \cdot \text{s}^{-1}$  and the tensile force is 3 N, the influence of the hollow capillary array on the shape and size of the whole multi-layer MCF is studied through numerical simulation.

- (1) After the MCF separates from the extrusion die, the shape of the capillary changes from circular to elliptical or oval. The central capillaries have a large ratio of width to depth, and the edge capillaries have a small ratio of width to depth. The aspect ratios of capillary change from 1.01 to 1.76.
- (2) With the same layers, when the two-dimensional hollow capillary array is aligned, the multi-layer MCF has a small aspect ratio of capillary and large film porosity. When the two-dimensional hollow capillary array is non-aligned, the MCF has a large aspect ratio of capillary and small film porosity.
- (3) In the four-layer MCF, if the capillary array is aligned, the aspect ratio of the capillaries is lower and the film porosity is higher. They are suitable for micro-reactors and melt pumps. In the three- and four-layer MCF, if the capillary arrays are non-aligned, the high aspect ratio of capillaries and higher film porosity will be obtained. Therefore, they are suitable for micro heat exchangers.

**Funding information:** This work was supported by the National Natural Science Foundation of China (NSFC) (No. 52063021). Grant Recipient: Jianhua Xiao.

**Author contributions:** Jianhua Xiao: writing – review and editing, supervision; Ru Yang: writing- original draft preparation, project administration; Shiqiang Song: conceptualization, methodology; Haibin Wang and Haiwei Wen: software, investigation.

**Conflict of interest:** The authors state no conflict of interest.

## Reference

- (1) Hallmark B, Hesketh RP, Hornung C, Mackley MR. The manufacture and hydraulic characterization of novel micro-capillary film (MCF) extrusions. Proceedings of the 1st International Symposium on Process Intensification and Miniaturization; 2003 Jan 22–24. UK: Newcastle; 2003.
- (2) Hallmark B, Mackley MR. The effect of polymer rheology and processing conditions on the manufacture of novel micro-capillary film (MCF) extrusions. Proceedings of the XIVth International Congress on Rheology; 2004 Aug 22–27. Seoul, Korea. Seoul: The Korean Society of Rheology; 2004.
- (3) Gerald B, David M, Joseph D, Tom P, Clifford T. Microcapillary film membranes based on polyvinylidene fluoride. ANTEC Conference; 2018 May 12–15. USA: Hilton Anaheim; 2018. <https://www.researchgate.net/publication/325575762>.
- (4) Hallmark B, Mackley MR, Gadala-Maria F. Hollow microcapillary arrays in thin plastic films. *Adv Eng Mater*. 2005;7(6):545–7. doi: 10.1002/adem.200400154.
- (5) Hornung CH, Hallmark B, Hesketh RP, Mackley MR. The fluid flow and heat transfer performance of thermoplastic microcapillary films. *J Micromech Microeng*. 2006;16(2):434–47. doi: 10.1088/0960-1317/16/2/030.
- (6) Hallmark B, Hornung CH, Broady D, Price-Kuehne C, Mackley MR. The application of plastic microcapillary films for fast transient micro-heat exchange. *Int J Heat Mass Transf*. 2008;51(21–22):5344–58. doi: 10.1016/j.ijheatmasstransfer.2008.01.036.
- (7) Dorfeling C, Hornung CH, Hallmark B, Beaumont RJJ, Fovargue H, Mackley MR. The experimental response and modelling of a solar heat collector fabricated from plastic microcapillary films. *Sol Energy Mat Sol Cells*. 2010;94(07):1207–21. doi: 10.1016/j.solmat.2010.03.008.
- (8) Hornung CH, Mackley MR, Baxendale IR, Ley SV. A microcapillary flow disc reactor for organic synthesis. *Org Process Res Dev*. 2007;11(3):399–405. doi: 10.1021/op700015f.
- (9) Gill KK, Gibson R, Yiu KHC, Hester P. Microcapillary film reactor outperforms single-bore mesocapillary reactors in continuous flow chemical reactions. *CEJ*. 2021;408(15):127860–71. doi: 10.1016/j.cej.2020.127860.
- (10) Barbosa AI, Barreto AS, Reis NM. Transparent, hydrophobic FEP Teflon offers rapid, robust and irreversible passive adsorption of diagnostic antibodies for sensitive optical biosensing. *ACS Applied Bio Materials*. 2019;2(7):2780–90. doi: 10.1021/acsabm.9b00214.
- (11) Moreira RPM, Puma GL. CFD modeling of pharmaceuticals and CECs removal by UV/H<sub>2</sub>O<sub>2</sub> process in helical microcapillary photoreactors and evaluation of OH radical rate constants. *CEJ*. 2021;415(07):128833–47. doi: 10.1016/j.cej.2021.128833.
- (12) Nicholas JD, Bart H, Pulkit A, James T, Vincent BH, Nigel KHS. On the magnetic field architecture required to capture superparamagnetic nanoparticles in a microcapillary flow. *J Nanopart Res*. 2010;12:307–17. doi: 10.1007/s11051-009-9615-0.
- (13) Marcus B, Ian RB, Steven VL. The flow synthesis of heterocycles for natural product and medicinal chemistry applications. *Mol Divers*. 2011;15:613–30. doi: 10.1007/s11030-010-9282-1.
- (14) Isabel PA, Nuno MR. Immunocapture of *Escherichia coli* in a fluoropolymer microcapillary array. *J Chromatogr A*. 2019;1585(25):46–55. doi: 10.1016/j.chroma.2018.11.067.
- (15) Zheyun X, Feng J, Fanghao Z, Zhongbin X, Haoyan X, Xiaodong R. Determination of hydrogen peroxide using novel test strips based on plastic microcapillary film. *Anal Methods-UK*. 2017;21:3230–6. doi: 10.1039/C7AY00584A.

- (16) Liu J, Xu Z, Shan Y, Huang X. Applications of microcapillary film in bioanalytical techniques. *Analyst*. 2021;5(01):1529–37. doi: 10.1039/D0AN01945C.
- (17) Alves IP, Reis NM. Microfluidic smartphone quantitation of *Escherichia coli* in synthetic urine. *Biosens Bioelectron*. 2019;145(09):111624–32. doi: 10.1016/j.bios.2019.111624.
- (18) Medina DI, Chinesta F, Mackley MR. Heat melding of voided polyethylene microstructures. *Polymer*. 2009;50(14):3302–10. doi: 10.1016/j.polymer.2009.04.051.
- (19) Hallmark B, Gadala-Maria F, Mackley MR. The melt processing of polymer microcapillary film (MCF). *J Non-Newton Fluid*. 2005;128(3):83–98. doi: 10.1016/j.jnnfm.2005.03.013.
- (20) Lamb H. *Hydrodynamics*. 6th edn. New York: Dover; 1945.